Sprague-Dawley Rats Bearing McA-RH7777 Cells for Study of Hepatoma and Transarterial Chemoembolization

HYE RIM CHO[1*], JIN WOO CHOI[1*], HYO-CHEOL KIM[1], YONG SUB SONG[1], GYOUNG MIN KIM[2], KYU RI SON[2] and JIN WOOK CHUNG[1]

[1]*Department of Radiology, Seoul National University College of Medicine, Institute of Radiation Medicine, Seoul National University Medical Research Center, and Clinical Research Institute, Seoul National University Hospital, Seoul, Korea;*
[2]*Department of Radiology, Korea University Anam Hospital, Korea University College of Medicine, Seoul, Korea*

Abstract. *Aim: To evaluate the feasibility of the McA-RH7777 tumor model in Sprague-Dawley (SD) rats, for study of hepatoma and transarterial chemoembolization. Materials and Methods: McA-RH7777 rat hepatoma cells (1×10^7) were inoculated into the left hepatic lobe of SD rats (n=38). Chemoembolization with left common carotid artery access was performed using an emulsion of iodized oil and doxorubicin, and polyvinyl alcohol particles. Tumor induction rate and response to chemoembolization were assessed by magnetic resonance imaging and histology. Results: Tumor induction rate of McA-RH7777 in SD rat livers was 73.3% (11/15). Hematoxylin-and-eosin staining revealed hypercellular tumor with a trabecular pattern that mimics human hepatocellular carcinoma. Chemoembolization was successfully conducted in all rats. There was a significant difference in tumor growth rates between the chemoembolization-treated and control groups ($p<0.0001$). Conclusion: A rat tumor model of McA-RH7777 cells in SD rats is feasible and has the potential to be a good model for hepatoma and chemoembolization studies.*

Animal models have been developed to enable understanding of the effects of transarterial chemoembolization and new therapeutic agents for hepatocellular carcinoma (HCC). The rabbit VX2 tumor model has been widely used for several decades because the size of the rabbit hepatic artery is appropriate for the introduction of microcatheters (1-3). However, VX2 tumor cells do not originate from hepatocytes (4), and biological studies such as, those using immunohistochemical staining, are limited in the rabbit model. For these reasons, rodent HCC models have been investigated in various studies of anticancer therapies (5-12). The two most common rodent HCC models are the Morris hepatoma model (McA-RH7777 cells in Buffalo rat) and the Novikoff hepatoma model [N1-S1 cells in Sprague-Dawley (SD) rats] (8-12). However, Buffalo rat is not widely available in some countries and is generally more expensive than SD rats, and N1-S1 cells in the SD rats have a suboptimal tumor induction rate (59-75%) (8-10). In addition, according to our experience, Novikoff hepatoma sometimes undergoes spontaneous regression.

In terms of anticancer therapies, several studies have been conducted on intra-arterial treatment in rodent HCC models, using a gastroduodenal artery approach after laparotomy (6-8), and a carotid artery approach with manual assistance after laparotomy (13). In addition, a femoral artery approach without laparotomy was recently reported as an alternative method for chemoembolization in rodent HCC models (14, 15). Nonetheless, the previous three methods have drawbacks in that the former two require laparotomy, which increases the procedure-related morbidity and mortality, whereas the latter technique has been tested with rather large-sized animals (14). Therefore, we believe that a more useful method to achieve chemoembolization in a rat hepatoma model is warranted.

Meanwhile, Dr. Larson of Northwestern University recently mentioned the tumorigenicity of McA-RH7777 cells in an SD rat (personal communication). Therefore, we attempted to evaluate a new hepatoma model in SD rats bearing McA-RH7777 cells, and to apply a new chemoembolization technique using only the common carotid artery approach without laparotomy in the rat

*These Authors contributed equally to this study.

Correspondence to: Hyo-Cheol Kim, MD, Department of Radiology, Seoul National University Hospital, # 28 Yongon-dong, Chongno-gu, Seoul, 110-744, Korea. Tel: +82 220722584, Fax: +82 27436385, e-mail: angiointervention@gmail.com

Key Words: Hepatocellular carcinoma, animal model, rat, chemoembolization.

hepatoma model. The aims of this study were to evaluate the feasibility of the McA-RH7777 tumor model in SD rats, and to assess the adequacy of the model for transarterial chemoembolization study, using a unilateral common carotid artery approach without laparotomy.

Materials and Methods

Tumor cell line. The McA-RH7777 rat hepatoma cell line (CRL-1601; ATCC, Manassas, VA, USA) was obtained and cultured in Dulbecco's modified Eagle's medium (DMEM; WelGENE, Daegu, Korea) supplemented with 10% fetal bovine serum (WelGENE) and 1% penicillin-streptomycin mixture (Gibco, Grand Island, NY, USA). McA-RH7777 cells were loosely adherent in culture flasks at 37˚C in a humidified atmosphere containing 5% CO_2. The viability of the cells was tested with trypan blue staining (confirming >90% cell viability for each tumor implantation procedure).

Animal model. The study was approved by our Institutional Animal Care and Use Committee, and performed in accordance with institutional guidelines. Thirty-eight male SD rats, initially weighing 300-350 g, were used for this study. SD rats were anesthetized by injecting a solution of zolazepam (5 mg/kg, Zoletil®; Virbac, Carros cedex, France) and xylazine (10 mg/kg, Rompun®; Bayer-Schering Pharma, Berlin, Germany) into the hindlimb. After anesthesia, a midline mini-laparotomy was performed and the left lateral hepatic lobe was exposed. McA-RH7777 rat hepatoma cells (1×10^7) were prepared in 50 μl of serum-free DMEM and gently injected under the hepatic capsule into the left lateral lobe. Handheld cautery (Bovie Medical Corporation, Clearwater, FL, USA) was applied to prevent bleeding and reflux of the cells, then the abdominal incisions were closed with a two-layer technique.

MRI and histological analysis. MRI was performed in a 3-Tesla clinical MRI unit (TrioTim; Siemens Medical Solutions, Erlangen, Germany) with a 6-channel rat body coil (Stark Contrast, Erlangen, Germany). We acquired axial T2-weighted turbo spin echo images (TR/TE, 3800/78 ms; 199 Hz/pixel bandwidth; flip angle of 140˚; slice thickness of 2 mm; field of view of 120×109 mm; 256×197 matrix). A radiology resident (J.W.C) selected an image slice scanned through the center of tumor, and measured the longest diameter of each hepatoma. Animals for chemoembolization study additionally underwent diffusion-weighted images with single-shot echo planar imaging (TR/TE, 2100/75 ms; 988 Hz/pixel bandwidth; slice thickness of 4 mm; field of view of 80×60 mm; 64×48 matrix, b-value=800 s/mm^2). To evaluate changes in apparent diffusion coefficient (ADC) values, which suggest changes in tissue cellularity, following chemoembolization, a radiology resident drew a circular region-of-interest (ROI) for each tumor. The ROIs on the ADC map were drawn as large as possible within the confines of each tumor, in consideration of T2-weighted images and diffusion-weighted images. All image analyses were conducted using an image archiving and communication system (Marosis, Marotech, Seoul, Korea).

All rats were euthanized in a CO_2 chamber for subsequent histological analysis. Axial sections sampled across the center of the tumor were fixed in 10% buffered formaldehyde solution and were paraffin embedded. Hematoxylin & eosin (H&E) staining was then performed on each sample.

Feasibility of tumor model. Fifteen SD rats out of 38 subjects were studied to assess the tumor induction rate and the natural course of our hepatoma model. Serial MRI (T2-weighted images) was obtained at 10, 17, and 24 days after tumor implantation. The rats were euthanized and tumors were sampled immediately after the last MRI.

Transarterial chemoembolization. The remaining 23 SD rats were utilized to test the adequacy of transarterial chemoembolization study in a new hepatoma model. Baseline MRI (T2-weighted images and diffusion-weighted images) was conducted 10 days after tumor implantation. According to baseline MRI, we selected subjects with hepatoma ≥10 mm for chemoembolization procedure.

One day after the baseline MRI, transarterial chemoembolization was performed by an experienced interventional radiologist (H. Kim). After anesthesia was achieved in the same manner for tumor implantation, the rats were placed on an angiography table, and the neck was shaved and cleansed with povidone iodine solution. A 2-cm longitudinal left paramedian incision was made in the neck. The left common carotid artery was exposed by dissecting the neck muscles and separating the carotid sheath. The distal common carotid artery was ligated using 3-0 Mersilk (Ethicon, Norderstedt, Germany) and a double-loop sling was formed around the proximal common carotid artery with 3-0 Mersilk. The common carotid artery was cannulated by a 22-gauge intravenous catheter. A 1.5 Fr microcatheter (Marathon; EV3, Irvine, CA) was shortened to 20-cm by removing the distal portion and reassembled with the hub onto the remaining microcatheter, and a 0.010-inch (0.0254 cm) guidewire (Silverspeed-10; EV3) was inserted through the cannula. During the procedure, the aforementioned sling was sufficiently tightened to prevent bleeding at the carotid artery entry site. Abdominal aortograms (Figure 1A) and celiac angiograms were obtained to identify the hepatic artery anatomy by manually injecting contrast media through the microcatheter. After inserting the guidewire into the left hepatic artery, the microcatheter was advanced into the proper or left hepatic artery (Figure 1B). An emulsion of 0.1 ml of iodized oil and 0.5 mg of doxorubicin hydrochloride was infused, and then additional embolization was performed by using polyvinyl alcohol particles of 45-150 μm in diameter (Contour®; Boston Scientific, Natick, MA, USA) (Figure 1C) (chemoembolization group). The microcatheter was then removed, and the carotid artery was ligated. The neck incision was sutured with a one-layer technique.

Follow-up MRI (T2-weighted images and diffusion-weighted images) was conducted 7 and 14 days (18 and 25 days from tumor implantation, respectively) after the chemoembolization procedure, using the same protocols as the baseline MRI. All rats were euthanized and tumors were sampled immediately after the last follow-up MR imaging.

Statistical analysis. Fifteen rats, used for studying the feasibility of the tumor model with hepatoma ≥10 mm on the first MRI (10 days from tumor implantation), were analyzed as the control group of the chemoembolization study. The experimental group of the chemoembolization study was defined as those rats that finally underwent transarterial chemoembolization procedure and survived until the last follow-up MRI, among the 23 candidate subjects. Based on tumor sizes on the first and the last MRI, the tumor growth rate was defined as follows:

$$\text{Tumor growth rate } \% = \frac{(\text{final tumor size}) - (\text{initial tumor size})}{(\text{initial tumor size})} \times 100$$

Figure 1. *Fluoroscopic images of transarterial chemoembolization via the left common carotid artery in a rat hepatoma model. A: Aortogram (lateral view) demonstrates the aorta, the celiac artery (arrowhead) and the proper hepatic artery (arrow), forming a U-shape. B: Hepatic angiogram presents staining of a round tumor (arrowheads). C: Spot image after chemoembolization shows accumulation of iodized oil in the tumor (arrowheads).*

The difference in tumor growth rates between the control and experimental groups was compared using the Mann-Whitney *U*-test. Additionally, as for subjects that received chemoembolization, changes in ADC values between the baseline and last follow-up MRI were evaluated using the Wilcoxon signed rank test.

A p-value <0.05 was considered to indicate statistical significance, and all statistical analyses were performed with commercially available software (SPSS 17.0; SPSS, Chicago, IL, USA).

Results

Feasibility of the tumor model. Fourteen out of 15 SD rats exhibited a T2 hyperintense lesion in the liver, which ranged from 4.5 mm to 15.4 mm, on the first MRI (10 days from tumor implantation). During the serial MRI follow-up, three tumors were found to have spontaneously regressed. Specifically, among four tumors <10 mm on the first MRI, three tumors (4.5 mm, 5.9 mm, and 7.0 mm) were not detected on the last MRI (24 days from tumor implantation), but the remaining tumor (7.0 mm) had grown to 12.0 mm on the final MRI. Therefore, the tumor induction rate of McA-RH7777 on SD rat liver was 73.3% (11/15) in our study. The final tumor size in the 11 rats ranged from 12.0 mm to 25.0 mm [mean±standard deviation (SD), 18.7±3.1 mm] on the last MRI. Peritoneal seeding was found in two subjects, and intrahepatic metastasis was noticed in another. H&E staining revealed a hypercellular tumor with trabecular pattern, mimicking human HCC (Figure 2).

Transarterial chemoembolization. Fifteen out of 23 SD rats exhibited a tumor ≥10 mm on baseline MRI, and were finally studied for transarterial chemoembolization. The mean±SD of tumor sizes and ADC values prior to chemoembolization were 13.3±5.2 mm and 721.2±67.9×10^{-6} mm^2/s, respectively. Transarterial chemoembolization with left common carotid artery approach was successfully performed in all 15 rats. One subject in which the tumor was 11 mm on the baseline MRI died the day after chemoembolization. However, the remaining 14 rats did not exhibit any complications, including neurological deficits. On the last follow-up MRI (25 days after tumor implantation), the mean±SD of tumor sizes and ADC values were 13.6±3.6 mm and 1598.3±57.5×10^{-6} mm^2/s, respectively. From the results of the Wilcoxon signed-rank test, there was a significant difference between ADC values of pre- and post-chemoembolization MRI (p=0.001) (Figure 3). H&E staining revealed either near total necrosis of the tumor or partial necrosis with marginal recurrence (Figure 3).

Tumor growth rate depending on chemoembolization. Tumor growth rate between 10 and 24 days after tumor implantation was 82.4±12.0% in 10 rats that did not undergo chemoembolization. Peritoneal seeding (n=2) and intrahepatic metastasis (n=1) were not taken into account in the calculation of the tumor growth rate. In contrast, the tumor growth rate between 10 and 25 days after tumor implantation was 3.7±11.4% in 14 subjects that received chemoembolization. From the results of the Mann-Whitney *U*-test, there was a significant difference in tumor growth rates between the two groups (p<0.0001).

Discussion

Over the past few decades, the VX2 tumor model in rabbits has been widely adopted in much research particularly in chemoembolization studies for HCC, despite many advantages in murine tumor models – for example, ease in breeding and handling of small animals, and the availability of diverse tools for biochemical analyses (1-3). The sufficiently large size of the systemic arteries in the rabbit partly explains the popularity of the VX2 tumor model. In comparison with smaller animals such as rats, the femoral artery of a rabbit is large enough to accommodate a 4 Fr sheath and a 2.0 Fr microcatheter, and the proper hepatic artery is relatively easy to be selected (16). Furthermore, it was recently shown that the rabbit ear artery can be utilized as an easier arterial access site due to the unique anatomy of rabbits (17). Nevertheless, the fact that VX2 tumor is not of hepatocellular origin and it lacks biochemical tools such as suitable antibodies for immunohistochemical staining has limited research with the rabbit model.

Therefore, the development of solid hepatoma models in small animals has been one of the major interests of many researchers. However, there are also limitations in the two most widespread rat models for establishing orthotopic hepatoma. The Morris hepatoma model with McA-RH7777 cells in Buffalo rat is not available in some countries and the Buffalo rat is relatively expensive than the more popular SD or Fischer rats. Furthermore, the Morris hepatoma model is rather highly malignant, inducing multiple intrahepatic metastases within 3-4 weeks after tumor implantation (9), which may not be suitable for studies that require long-term follow-up. On the other hand, the Novikoff hepatoma model with N1-S1 cells in SD rats has a relatively low tumor induction rate compared with the Morris hepatoma model (9). Additionally, in terms of histology, the solid sheet pattern of Novikoff hepatoma is a less adequate histological model for human HCC, compared with the trabecular pattern of Morris hepatoma (9).

In contrast, our tumor model with McA-RH7777 in SD rats presented a higher, or at least comparable tumor induction rate, compared with that of the Novikoff hepatoma model (73.3% *vs*. 59-75%, respectively) (8-10). In addition, our study revealed that only 27.3% (3/11) of hepatomas exhibited peritoneal seeding or intrahepatic metastasis during the initial 24 days from tumor implantation, which suggests that our tumor model is less malignant than that of Morris hepatoma

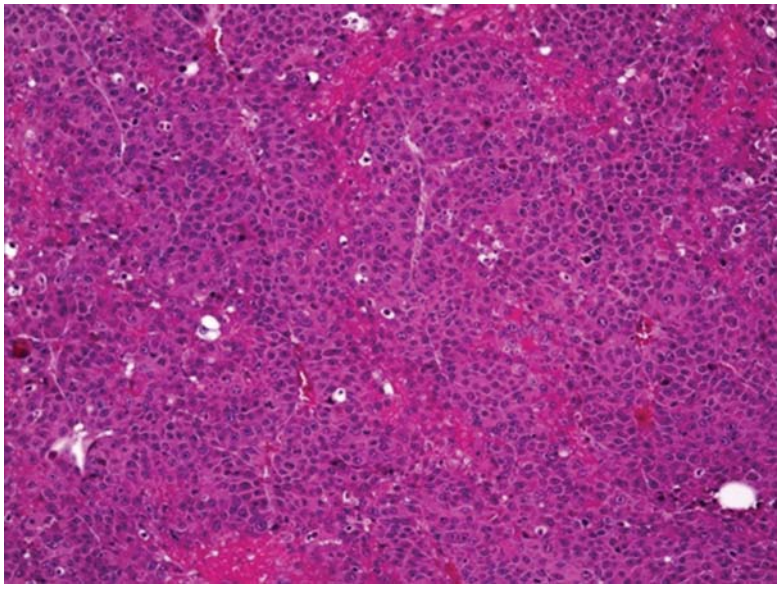

Figure 2. *Hematoxylin and eosin staining (magnification, ×100) of McA-RH7777 tumor implanted in a Sprague-Dawley rat shows a trabecular histological pattern that is similar to histology of human hepatocellular carcinoma.*

and may be more appropriate for studies needing long term follow-up. The trabecular histological pattern of the tumor indicates this model is also a good mimicker of human HCC in the histological aspect. Furthermore, McA-RH7777 implanted in SD rats responded well to chemoembolization, demonstrating either near total necrosis of the tumor, or partial necrosis with marginal recurrence. Moreover, the significant increase in ADC values after chemoembolization is consistent with previous human studies on chemoembolization and diffusion-weighted MRI (18, 19). These features suggest that our tumor model has more than adequate potential as a good model for chemoembolization study.

Moreover, we successfully performed transarterial chemoembolization *via* the left common carotid artery of SD rats, without additional laparotomy. We believe this approach to be safer, as well as easier than any other method used for chemoemblization in rat hepatoma models. Although Ju *et al*. reported no hindlimb ischemia after a transfemoral approach (14), ligation of the femoral artery at the end of the procedure may be more risky than ligation of the common carotid artery in rats. The presumption is based on the anatomical difference between the femoral and common carotid arteries. Specifically, autoregulatory vasodilatation and redistribution of cerebral blood flow through the collateral vasculature are able to minimize neurological complications after ligation of the unilateral common carotid artery (20, 21), while the femoral artery is anatomically classified as an end artery, lacking well-developed collaterals. Concordantly, it is reported that unilateral common carotid artery ligation in rats causes only minor alteration in cerebral blood flow and metabolism in the ipsilateral hemisphere (20, 22). In addition, the celiac artery initially courses downwards as it arises from the aorta and then the common hepatic artery courses upwards, thus forming a U-shaped course (Figure 1A). This is why the reverse-shaped catheter is commonly used for chemoembolization in humans. However, it is impossible to apply the same technique in rats due to the small caliber of the rat aorta. Therefore, the common carotid access offers a more favorable angle for engagement of the celiac artery with a microcatheter than does the transfemoral approach.

In conclusion, a tumor model of McA-RH7777 cells in SD rats is feasible and has potential to be a good model for chemoembolization studies. In addition, hepatic artery catheterization *via* the common carotid artery may be a safer as well, as easier, technique to achieve chemoembolization in rat hepatoma models.

Conflicts of Interest

The Authors declare that they have no conflicts of interest.

Acknowledgements

The Authors thank Yang Guo and Andrew C. Larson of Northwestern University, for their advice in this study.

This study was supported by Basic Science Research Program through the National Research Foundation of Korea (NRF) funded by the Ministry of Education, Science and Technology (2010-0010788).

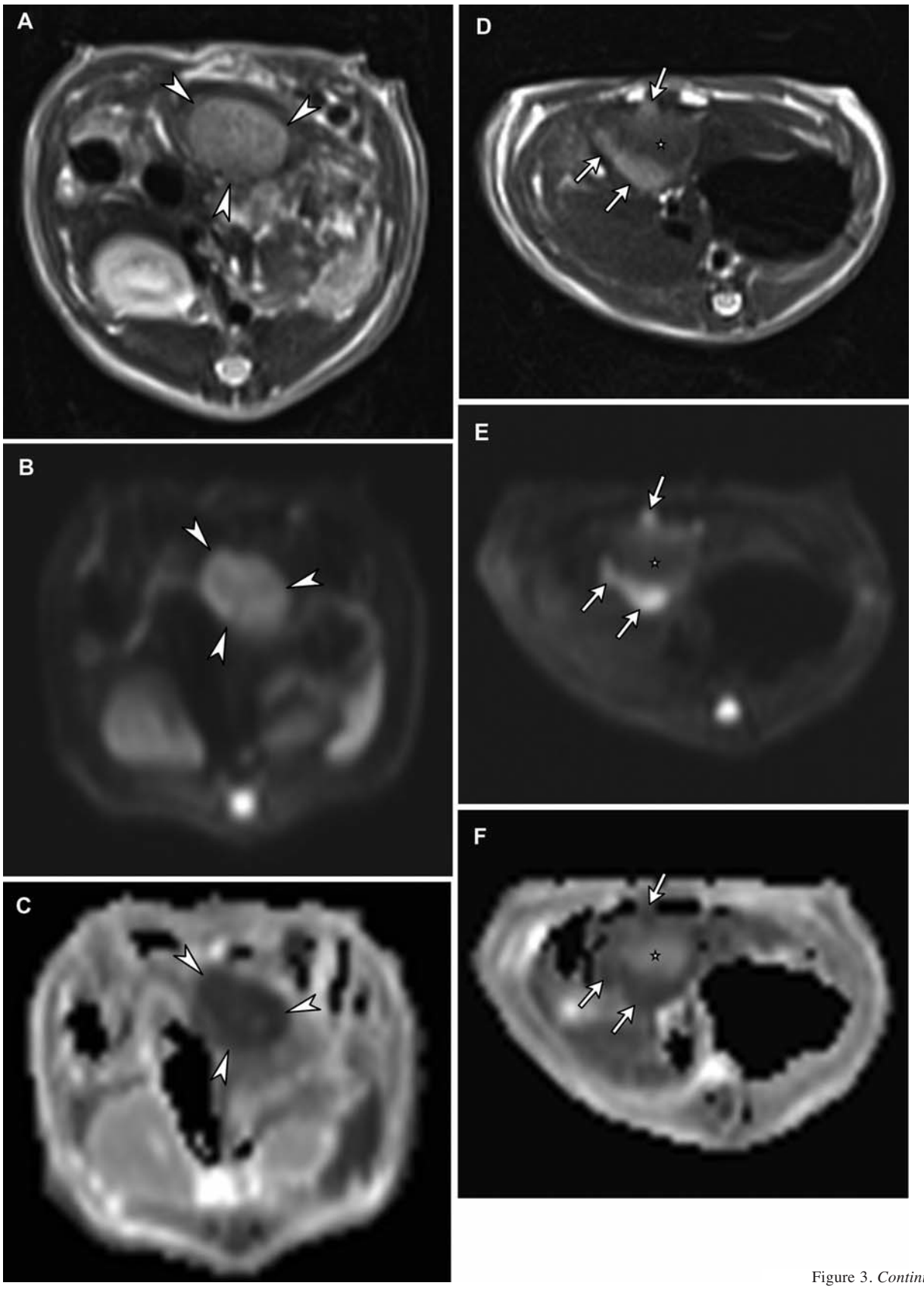

Figure 3. *Continued*

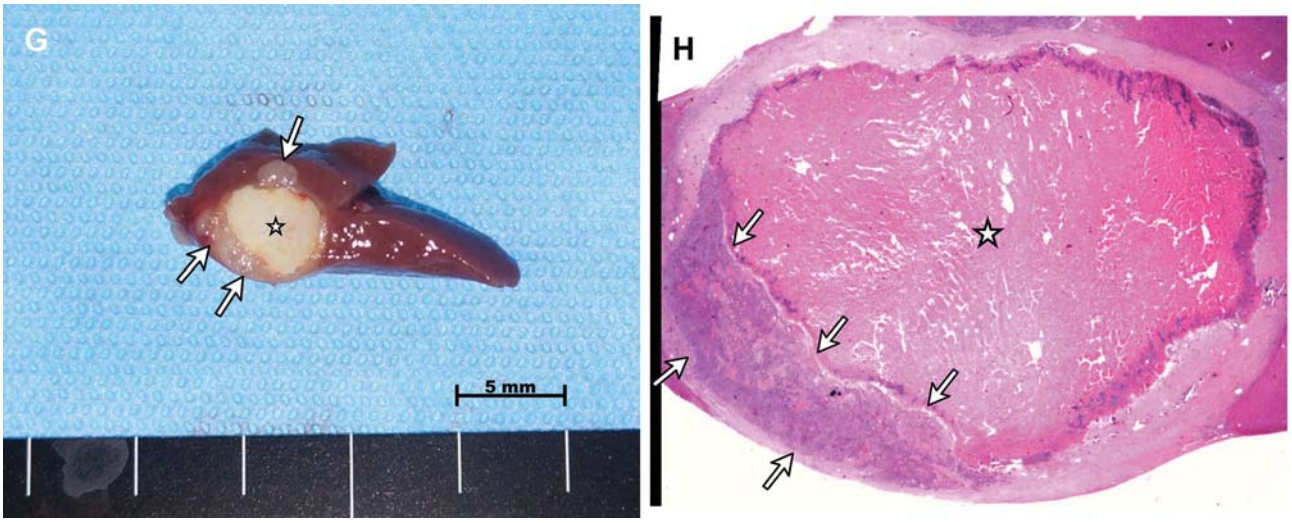

Figure 3. *Representative findings in MRI and histology in the chemoembolization group of our tumor model. The rat underwent baseline MRI study, chemoembolization, and follow-up MRI study at 10, 11, and 25 days from tumor implantation, respectively. A: Baseline axial T2-weighted MRI depicts a 1.2-cm, well-defined tumor in the left lateral lobe of the liver. B: Baseline axial diffusion-weighted MR image (echo planar imaging, b-value=800 s/mm^2) demonstrates hyperintensity of the tumor. C: Baseline axial apparent diffusion coefficient (ADC) map concordantly shows marked diffusion restriction (mean ADC value, 727×10^{-6} mm^2/s) of the tumor, which suggests hypercellularity of the tumor. D: Follow-up axial T2-weighted MRI depicts central hypointense region (asterisk) and peripheral hyperintense ares (arrows). E: Follow-up axial diffusion-weighted MRI (echo planar imaging, b-value=800 s/mm^2) demonstrates central hyperintense region (asterisk) and peripheral hyperintense areas (arrows). F: Follow-up axial ADC map shows concordant high water diffusivity in the central region (asterisk) and marked diffusion restriction in the peripheral portions (arrows). G: Gross specimen of the tumor shows findings compatible to those of the MRI, that is, central necrosis (asterisk) and peripheral viable tumor cells (arrows). H: Hematoxylin and eosin staining (magnification, ×12.5) of the tumor also reveals substantial necrosis in the tumor center (asterisk) and viable tumor cells in the periphery (arrows).*

References

1 Burgener FA: Peripheral hepatic artery embolization in rabbits with VX2 carcinomas of the liver. Cancer *46(1)*: 56-63, 1980.

2 Geschwind JF, Artemov D, Abraham S, Omdal D, Huncharek MS, McGee C, Arepally A, Lambert D, Venbrux AC and Lund GB: Chemoembolization of liver tumor in a rabbit model: Assessment of tumor cell death with diffusion-weighted MR imaging and histologic analysis. J Vasc Interv Radiol *11(10)*: 1245-1255, 2000.

3 Wang Y, Zheng C, Liang B, Zhao H, Qian J, Liang H and Feng G: Hepatocellular necrosis, apoptosis, and proliferation after transcatheter arterial embolization or chemoembolization in a standardized rabbit model. J Vasc Interv Radiol *22(11)*: 1606-1612, 2011.

4 Osato T and Ito Y: *In vitro* cultivation and immunofluorescent studies of transplantable carcinomas Vx2 and Vx7. Persistence of a Shope virus-related antigenic substance in the cells of both tumors. J Exp Med *126(5)*: 881-886, 1967.

5 Wu L, Tang ZY and Li Y: Experimental models of hepatocellular carcinoma: developments and evolution. J Cancer Res Clin Oncol *135(8)*: 969-981, 2009.

6 Jiang H, Meng Q, Tan H, Pan S, Sun B, Xu R and Sun X: Antiangiogenic therapy enhances the efficacy of transcatheter arterial embolization for hepatocellular carcinomas. Int J Cancer *121(2)*: 416-424, 2007.

7 Hanada M, Baba A, Tsutsumishita Y, Noguchi T, Yamaoka T, Chiba N and Nishikaku F: Intra-hepatic arterial administration with miriplatin suspended in an oily lymphographic agent inhibits the growth of tumors implanted in rat livers by inducing platinum–DNA adducts to form and massive apoptosis. Cancer Chemother Pharmacol *64(3)*: 473-483, 2009.

8 Garin E, Denizot B, Roux J, Noiret N, Lepareur N, Moreau M, Mesba H, Laurent JF, Herry JY, Bourguet P, Benoit JP and Lejeune JJ: Description and technical pitfalls of a hepatoma model and of intra-arterial injection of radiolabelled lipiodol in the rat. Lab Anim *39(3)*: 314-320, 2005.

9 Guo Y, Klein R, Omary RA, Yang GY and Larson AC: Highly malignant intra-hepatic metastatic hepatocellular carcinoma in rats. Am J Transl Res *3(1)*: 114-120, 2010.

10 Guo Y, Zhang Y, Klein R, Nijm GM, Sahakian AV, Omary RA, Yang GY and Larson AC: Irreversible electroporation therapy in the liver: Longitudinal efficacy studies in a rat model of hepatocellular carcinoma. Cancer Res *70(4)*: 1555-1563, 2010.

11 Zheng Z, Park SY, Lee M, Phark S, Won NH, Kang HS and Sul D: Effects of benzo(a)pyrene on the expression of heat shock proteins, pro-inflammatory cytokines and antioxidant enzymes in hepatic tumors induced by rat hepatoma N1-S1 cells. J Korean Med Sci *26(2)*: 222-230, 2011.

12 Altomonte J, Braren R, Schulz S, Marozin S, Rummeny EJ, Shmid RM and Ebert O: Synergistic antitumor effects of transarterial viroembolization for multifocal hepatocellular carcinoma in rats. Hepatology *48(6)*: 1864-1873, 2008.

13 Li X, Wang YX, Zhou X, Guan Y and Tang C: Catheterization of the hepatic artery *via* the left common carotid artery in rats. Cardiovasc Intervent Radiol *29(6)*: 1073-1076, 2006.

14 Ju S, McLennan G, Bennett SL, Liang Y, Bonnac L, Pankiewicz KW and Jayaram HN: Technical aspects of imaging and transfemoral arterial treatment of N1-S1 tumors in rats: An appropriate model to test the biology and therapeutic response to transarterial treatments of liver cancers. J Vasc Interv Radiol *20(3)*: 410-414, 2009.

15 Thompson SM, Callstrom MR, Knudsen B, Anderson JL, Carter RE, Grande JP, Roberts LR and Woodrum DA: Development and preliminary testing of a translational model of hepatocellular carcinoma for MR imaging and interventional oncologic investigations. J Vasc Interv Radiol *23(3)*: 385-395, 2012.

16 Kim HC, Chung JW, Choi SH, Im SA, Yamasaki Y, Jun S, Jae HJ and Park JH: Augmentation of chemotherapeutic infusion effect by TSU-68, an oral targeted antiangiogenic agent, in a rabbit VX2 liver tumor model. Cardiovasc Intervent Radiol *35(1)*: 168-175, 2012.

17 Chang IS, Lee MW, Kim YI, Choi SH, Kim HC, Choi YW, Yoon CJ, Shin SW and Lim HK: Comparison between transauricular and transfemoral arterial access for hepatic artery angiography in a rabbit model. J Vasc Interv Radiol *22(8)*: 1181-1187, 2011.

18 Chen CY, Li CW, Kuo YT, Jaw TS, Wu DK, Jao JC, Hsu JS and Liu GC: Early response of hepatocellular carcinoma to transcatheter arterial chemoembolization: choline levels and MR diffusion constants–initial experience. Radiology *239(2)*: 448-456, 2006.

19 Kamel IR, Liapi E, Reyes DK, Zahurak M, Bluemke DA and Geschwind JF: Unresectable hepatocellular carcinoma: Serial early vascular and cellular changes after transarterial chemoembolization as detected with MR imaging. Radiology *250(2)*: 466-473, 2009.

20 De Ley G, Nshimyumuremyi JB and Leusen I: Hemispheric blood flow in the rat after unilateral common carotid occlusion: Evolution with time. Stroke *16(1)*: 69-73, 1985.

21 Coyle P and Panzenbeck MJ: Collateral development after carotid artery occlusion in Fischer 344 rats. Stroke *21(2)*: 316-321, 1990.

22 Bronner G, Mitchell K and Welsh FA: Cerebrovascular adaptation after unilateral carotid artery ligation in the rat: Preservation of blood flow and ATP during forebrain ischemia. J Cereb Blood Flow Metab *18(1)*: 118-121, 1998.

Received October 23, 2012
Revised November 5, 2012
Accepted November 5, 2012